A NOTE ON A DISCONTINUOUS GALERKIN METHOD FOR RADIATION–DIFFUSION

ILARIA PERUGIA[†], DOMINIK SCHÖTZAU[‡], AND JAMES WARSA[§,¶]

Abstract. In recent papers, Warsa, Wareing and Morel introduced a mixed discontinuous finite element method for the discretization of a first order system of equations that describe the diffusion of radiation in materials. We show that this method belongs to the general class of discontinuous Galerkin methods studied by Castillo, Cockburn, Perugia, and Schötzau in [2]. Degree $k \geq 0$ polynomials are used to approximate the two unknowns appearing in the mixed formulation, the same degree being used for both. The method delivers convergence in the energy norm of order $k+\frac{1}{2}$ and convergence of the scalar flux in the L^2-norm of order $k+1$. The sharpness of these results is confirmed by numerical experiments for three dimensional model problems on tetrahedral meshes.

Key words. Discontinuous Galerkin methods, mixed finite element methods, radiation-diffusion

AMS subject classifications. 65N12, 65N30, 85A25, 85D75

1. Introduction. Over the last few years, discontinuous Galerkin (DG) methods have been successfully applied to a wide variety of problems; see the state–of–the–art surveys [3, 5, 7]. These methods are based on completely discontinuous finite element spaces combining finite element and finite volume technologies by using the ideas of numerical fluxes and slope limiters. This results in robust and high–order accurate schemes that can easily handle complicated geometries and boundaries. Moreover, DG methods are locally conservative – a desirable property for numerical solutions – because they weakly enforce conservation in an element–by–element fashion. In addition, such methods are well suited for the discretization of multi–physics and multi–material problems because they provide a single finite element framework for discretizing both diffusive and convective transport terms.

Recently, Warsa, Wareing and Morel introduced a discontinuous finite element method for the discretization of a radiation–diffusion problem in two– and three–dimensional domains; see [12] and [11]. It is represented by a system of two coupled first order equations for the zeroth and first angular moments of the angular flux (the direction–dependent solution to the Boltzmann transport equation). These equations are called the P_1 equations. They arise out of an angular Galerkin approximation to the Boltzmann transport equation based upon a spherical–harmonic trial space of first order; see [8] or [9] for more details. As in standard, upwind Godunov methods, their method conserves both the radiation energy and the radiation momentum over each cell. In combination with efficient preconditioning techniques, the results in [12, 13] indicate that the method of Warsa, Wareing and Morel can be effectively applied to a wide range of problems.

In this note, we show that the discrete formulation of the P_1 equations of Warsa, Wareing and Morel in fact belongs to the general class of mixed DG methods analyzed in [2]. This class extends and generalizes the local discontinuous Galerkin (LDG)

[†]Dipartimento di Matematica, Università di Pavia, Via Ferrata 1, 27100 Pavia, Italy; email: perugia@dimat.unipv.it.

[‡]Department of Mathematics, University of Basel, Rheinsprung 21, 4051 Basel, Switzerland; email: schotzau@math.unibas.ch.

[§]Transport Methods Group, Los Alamos National Laboratory, Los Alamos, NM 87545, USA; email: warsa@lanl.gov

[¶]This author's work is supported by the U. S. Department of Energy.

method proposed by Cockburn and Shu in [6] and further analyzed, in the context of pure diffusion problems, in [1, 4, 10]. Whereas in the original LDG approach the vector unknown can be eliminated from the equations in a local and element–wise manner, in the method of Warsa, Wareing and Morel, that belongs to the "truly" mixed variants of the LDG method described in [2], such a local elimination is no longer possible. While some may see this as a shortcoming of truly mixed DG methods, it does in fact lead to better and nearly optimal convergence rates for the approximation of the vector variable; see [2].

The theoretical results in [2] can then be applied to the method of Warsa, Wareing and Morel to show that the method is well–posed and to calculate a priori error bounds. For an approximation order $k \geq 0$, the method exhibits convergence rates in the mesh size of order $k + \frac{1}{2}$ in a suitable energy norm, and of order $k + 1$ in the L^2–norm of the scalar flux. The sharpness of these theoretical results is tested in a series of numerical experiments for a three dimensional model problem on tetrahedral meshes. These tests also complete the tests in [2] where no numerical results were shown for truly mixed DG methods.

The rest of the note is organized as follows. In section 2, we detail the radiation–diffusion problem that constitutes the P_1 equations. The precise formulation of the discontinuous Galerkin method under consideration is given in section 3. For the sake of completeness, we report in section 4 the main steps of the error analysis, following [2]. Section 5 shows the results of a numerical study supporting the theoretical results in section 4. The note concludes with some summary remarks in section 6.

2. The radiation–diffusion problem. The radiation–diffusion problem we consider in this work represents an angular Galerkin approximation to the linear Boltzmann transport equation that is based on a spherical–harmonic trial space of first order for the angular flux [8, 9]. This approximation comprises the so–called P_1 equations, a system of two first–order linear differential equations for the zeroth and first angular moments of the particle distribution (the scalar flux and current, respectively). Note that in the absence of time dependence (the case considered here) the two equations can be reduced to a single second order equation for one of the variables. It is the second order diffusion equation for the scalar flux that is typically used for accelerating or preconditioning radiation transport calculations [9], in contrast to the first order form presented in [11] and analyzed here.

Let $\Omega \subset \mathbb{R}^d$, $d = 2, 3$, be a bounded polygonal or polyhedral domain, whose boundary $\Gamma = \partial\Omega$ is partitioned into two parts $\Gamma = \Gamma_V \cup \Gamma_R$ with disjoint interiors. The problem is to find a solution that consists of the current $\mathbf{J} = \mathbf{J}(\mathbf{x})$ and scalar flux $\Phi = \Phi(\mathbf{x})$ satisfying the differential equations

$$\nabla \Phi + 3\,\sigma_t(\mathbf{x})\mathbf{J} = 3\,\mathbf{Q}_1, \qquad \nabla \cdot \mathbf{J} + \sigma_a(\mathbf{x})\Phi = Q_0, \tag{2.1}$$

subject to vacuum and reflecting boundary conditions

$$\frac{1}{4}\Phi - \frac{1}{2}\mathbf{J} \cdot \mathbf{n} = 0 \quad \text{on } \Gamma_V, \qquad \mathbf{J} \cdot \mathbf{n} = 0 \quad \text{on } \Gamma_R, \tag{2.2}$$

respectively, where $\mathbf{n}$ denotes the outward normal unit vector to Γ.

Here, $Q_0 \in L^2(\Omega)$ and $\mathbf{Q}_1 \in L^2(\Omega)^d$ are the zeroth and first angular moments of an inhomogeneous source. Furthermore, we assume the material coefficients σ_t and σ_a belong to $L^\infty(\Omega)$ and satisfy $\sigma_t(\mathbf{x}) \geq \sigma_\star > 0$ and $\sigma_a(\mathbf{x}) \geq 0$ in Ω ($\sigma_a = 0$ in purely scattering subregions). For simplicity, we also assume $\int_{\Gamma_V} ds > 0$ and exclude the pure Neumann case, $\Gamma_V = 0$.

3. Discontinuous Galerkin discretization. In this section, we detail the mixed discontinuous Galerkin discretization proposed by Warsa, Wareing and Morel [11, 12] and cast the method in the setting of [2].

3.1. Meshes and traces. We consider shape regular meshes $\mathcal{T}_h$ that partition the domain Ω into triangle and/or parallelograms, if $d = 2$, or tetrahedra and/or parallelepipeds, if $d = 3$, with possible hanging nodes. We denote by h_K the diameter of the element $K \in \mathcal{T}_h$ and set $h = \max_K h_K$. An *interior face* of $\mathcal{T}_h$ is defined as the (non–empty) $(d-1)$–dimensional interior of $\partial K^+ \cap \partial K^-$, where K^+ and K^- are two adjacent elements of $\mathcal{T}_h$, not necessarily matching. A *boundary face* of $\mathcal{T}_h$ is defined as the (non–empty) $(d-1)$–dimensional interior of $\partial K \cap \Gamma$, where K is a boundary element of $\mathcal{T}_h$. We assume that a boundary face belongs entirely either to Γ_V or Γ_R, respectively. We denote by $\mathcal{E}_\mathcal{I}$ the union of all interior faces of $\mathcal{T}_h$, by $\mathcal{E}_V$ and $\mathcal{E}_R$ the union of all boundary faces of $\mathcal{T}_h$ on Γ_V and Γ_R, respectively, and set $\mathcal{E} = \mathcal{E}_\mathcal{I} \cup \mathcal{E}_V \cup \mathcal{E}_R$.

For piecewise smooth vector– and scalar–valued functions $\mathbf{w}$ and u, we introduce the following trace operators. Let $e \subset \mathcal{E}_\mathcal{I}$ be an interior face shared by two elements K^+ and K^-, and write $\mathbf{n}^\pm$ for the outward normal unit vectors to the boundaries $\partial K^\pm$, respectively. Denoting by $\mathbf{w}^\pm$ and $u^\pm$ the traces on $\partial K^\pm$ taken from $K^\pm$, respectively, we define the *jumps* across e

$$[\![\mathbf{w}]\!] = \mathbf{w}^+ \cdot \mathbf{n}^+ + \mathbf{w}^- \cdot \mathbf{n}^-, \qquad [\![u]\!] = u^+ \mathbf{n}^+ + u^- \mathbf{n}^-,$$

and the *averages* $\{\!\{\mathbf{w}\}\!\} = (\mathbf{w}^+ + \mathbf{w}^-)/2$ and $\{\!\{u\}\!\} = (u^+ + u^-)/2$. On a boundary face $e \subset \mathcal{E}_V \cup \mathcal{E}_R$, we set $[\![\mathbf{w}]\!] = \mathbf{w} \cdot \mathbf{n}$, $[\![u]\!] = u\,\mathbf{n}$, $\{\!\{\mathbf{w}\}\!\} = \mathbf{w}$ and $\{\!\{u\}\!\} = u$.

3.2. Definition of the method. Let $\mathcal{T}_h$ be a triangulation $\mathcal{T}_h$ of Ω. We assume that the exact solution $(\mathbf{J}, \Phi)$ belongs to $\mathbf{W} \times U$, where

$$\begin{aligned} \mathbf{W} &= \{\, \mathbf{w} \in L^2(\Omega)^d \ : \ \mathbf{w}|_K \in H^1(K)^d,\ K \in \mathcal{T}_h\}, \\ U &= \{\, u \in L^2(\Omega) : \ u|_K \in H^1(K),\ K \in \mathcal{T}_h\}. \end{aligned}$$

We wish to approximate $(\mathbf{J}, \Phi)$ by discrete functions $(\mathbf{J}_h, \Phi_h) \in \mathbf{W}_h \times U_h$, where

$$\begin{aligned} \mathbf{W}_h &= \{\, \mathbf{w} \in L^2(\Omega)^d : \ \mathbf{w}|_K \in \mathcal{P}^k(K)^d,\ K \in \mathcal{T}_h\}, \\ U_h &= \{\, u \in L^2(\Omega) : \ u|_K \in \mathcal{P}^k(K),\ K \in \mathcal{T}_h\}, \end{aligned}$$

for $k \geq 0$, with $\mathcal{P}^k(K)$ denoting the set of polynomials of degree at most k on K, if K is a triangle or a tetrahedron, or the set of polynomials of degree at most k in each variable on K, if K is a parallelogram or a parallelepiped. This approximation is defined by imposing that, for all elements $K \in \mathcal{T}_h$ and all discrete test functions $(\mathbf{w}, u) \in \mathbf{W}_h \times U_h$,

$$\begin{aligned} &3 \int_K \sigma_t\, \mathbf{J}_h \cdot \mathbf{w}\, d\mathbf{x} - \int_K \Phi_h\, \nabla \cdot \mathbf{w}\, d\mathbf{x} + \int_{\partial K} \widehat{\Phi}_h\, \mathbf{w} \cdot \mathbf{n}_K\, ds = 3 \int_K \mathbf{Q}_1 \cdot \mathbf{w}\, d\mathbf{x}, \\ &- \int_K \mathbf{J}_h \cdot \nabla u\, d\mathbf{x} + \int_{\partial K} u\, \widehat{J}_{h,K}\, ds + \int_K \sigma_a\, \Phi_h\, u\, d\mathbf{x} = \int_K Q_0\, u\, d\mathbf{x}. \end{aligned} \tag{3.1}$$

Here, $\widehat{J}_{h,K}$ and $\widehat{\Phi}_h$ are the so–called *numerical fluxes*, that are approximations to the traces on the element interfaces of $\mathbf{J} \cdot \mathbf{n}_K$ and Φ and are chosen as follows (see [11]).

First, for an element K^+ and an interior face e shared by K^+ and a neighboring element K^-, we define the following inwardly and outwardly directed discrete flows

(partial currents) by

$$J^{\rm in}_{e,K^+} = \frac{1}{4}\Phi_h^- - \frac{1}{2}\mathbf{J}_h^- \cdot \mathbf{n}_{K^+}, \qquad J^{\rm out}_{e,K^+} = \frac{1}{4}\Phi_h^+ + \frac{1}{2}\mathbf{J}_h^+ \cdot \mathbf{n}_{K^+}.$$

If the face e of K^+ is contained in $\mathcal{E}_V \cup \mathcal{E}_R$, the outwardly directed flow $J^{\rm out}_{e,K^+}$ is defined as before. Further, if the face e of K^+ belongs to $\mathcal{E}_V$, we set $J^{\rm in}_{e,K^+} = 0$, whereas $J^{\rm in}_{e,K^+}$ is not needed for $e \subset \mathcal{E}_R$.

The numerical fluxes are then chosen as

$$\widehat{J}_{h,K}|_e = (1-\xi)\,(J^{\rm out}_{e,K} - J^{\rm in}_{e,K}), \qquad \widehat{\Phi}_h|_e = 2\left[(1+\xi)\,J^{\rm out}_{e,K} + (1-\xi)\,J^{\rm in}_{e,K}\right], \tag{3.2}$$

with $\xi = 0$, if $e \subset \mathcal{E}_{\mathcal{I}} \cup \mathcal{E}_V$, and $\xi = 1$, if $e \subset \mathcal{E}_R$.

This completes the definition of the DG method proposed in [11, 12] for problem (2.1)–(2.2) (where only the case $k = 1$ was considered because of the context in which the solution to the P_1 equations was applied). Notice that, for e shared by K^+ and K^-, $\widehat{J}_{h,K^+}|_e = -\widehat{J}_{h,K^-}|_e$, whereas the definition $\widehat{\Phi}_h|_e$ does not depend on which side of e it is taken from. This is the reason for the subscript K in $\widehat{J}_{h,K}$.

Let us now cast the fluxes in (3.2) in the setting of [2]. To this end, we denote by $\widehat{\mathbf{J}}_h$ a vector field such that $\widehat{\mathbf{J}}_h|_e \cdot \mathbf{n}_K = \widehat{J}_{h,K}$, for all $e \subset \partial K$ (the definition of $\widehat{\mathbf{J}}_h|_e$ no longer depends on which side it is taken from). Then we have that

$$\begin{aligned}
&\widehat{\mathbf{J}}_h|_e = \{\!\{\mathbf{J}_h\}\!\} + \frac{1}{4}[\![\Phi_h]\!], \quad &&\widehat{\Phi}_h|_e = \{\!\{\Phi_h\}\!\} + [\![\mathbf{J}_h]\!], \quad &&\text{if } e \subset \mathcal{E}_{\mathcal{I}},\\
&\widehat{\mathbf{J}}_h|_e = \frac{1}{2}\mathbf{J}_h + \frac{1}{4}\Phi_h\,\mathbf{n}, \quad &&\widehat{\Phi}_h|_e = \frac{1}{2}\Phi_h + \mathbf{J}_h \cdot \mathbf{n}, \quad &&\text{if } e \subset \mathcal{E}_V,\\
&\widehat{\mathbf{J}}_h|_e = \mathbf{0}, &&\widehat{\Phi}_h|_e = \Phi_h + 2\,\mathbf{J}_h \cdot \mathbf{n}, \quad &&\text{if } e \subset \mathcal{E}_R.
\end{aligned}$$

We point out that these fluxes are consistent, local and conservative in the sense of [1].

The above method belongs to the general class of mixed DG methods investigated in [2] and the theoretical results there can be used to analyze the method. In particular, the method is very similar to the original LDG method. Unlike for the LDG method, it is not possible to eliminate the unknown $\mathbf{J}_h$, element–by–element, in favor of the unknown Φ_h. On the other hand, the method here gives better orders of convergence for the unknown $\mathbf{J}_h$ than the original LDG method.

REMARK 3.1. *The choice in (3.2) of the numerical fluxes can be motived by physical arguments corresponding to the so–called Marshak approximation; see [11, 12] for details. Another possible approach for defining the numerical fluxes is closely associated with Riemann solvers used in the numerical solution of fluid dynamics problems. These alternate definitions are presented in [11]. There is no advantage in choosing one over the other, other than the context in which the P_1 equations will be applied. The results presented in this note are independent of this choice and we work with the Marshak approach here. Note that in either case, the numerical fluxes can be easily adapted to take into account inhomogeneous boundary data.*

3.3. Mixed setting. In this section, we rewrite the method as a classical (stabilized) mixed method. In order to do that, we sum (3.1) over all elements and obtain

$$\begin{aligned}
&3\int_\Omega \sigma_t\,\mathbf{J}_h \cdot \mathbf{w}\,d\mathbf{x} - \int_\Omega \Phi_h\,\nabla_h \cdot \mathbf{w}\,d\mathbf{x} + \int_{\mathcal{E}} \widehat{\Phi}_h\,[\![\mathbf{w}]\!]\,ds = 3\int_\Omega \mathbf{Q}_1 \cdot \mathbf{w}\,d\mathbf{x},\\
&-\int_\Omega \mathbf{J}_h \cdot \nabla_h u\,d\mathbf{x} + \int_{\mathcal{E}} \widehat{\mathbf{J}}_h \cdot [\![u]\!]\,ds + \int_\Omega \sigma_a\,\Phi_h\,u\,d\mathbf{x} = \int_\Omega Q_0\,u\,d\mathbf{x},
\end{aligned}$$

for all $(\mathbf{w}, u) \in \mathbf{W}_h \times U_h$, where $\nabla_h \cdot$ and ∇_h denote the element-wise divergence and gradient operators, respectively.

We introduce the bilinear forms

$$a(\mathbf{J}, \mathbf{w}) = 3 \int_\Omega \sigma_t \, \mathbf{J} \cdot \mathbf{w} \, d\mathbf{x} + \int_{\mathcal{E}_\mathcal{I} \cup \mathcal{E}_V} [\![\mathbf{J}]\!][\![\mathbf{w}]\!] \, ds + 2 \int_{\mathcal{E}_R} (\mathbf{J} \cdot \mathbf{n}) \, (\mathbf{w} \cdot \mathbf{n}) \, ds,$$
$$b(\mathbf{w}, u) = - \int_\Omega u \, \nabla_h \cdot \mathbf{w} \, d\mathbf{x} + \int_{\mathcal{E}_\mathcal{I} \cup \mathcal{E}_R} \{\!\{u\}\!\} [\![\mathbf{w}]\!] \, ds + \frac{1}{2} \int_{\mathcal{E}_V} u \, \mathbf{w} \cdot \mathbf{n} \, ds,$$
$$c(\Phi, u) = \int_\Omega \sigma_a \, \Phi \, u \, d\mathbf{x} + \frac{1}{4} \int_{\mathcal{E}_\mathcal{I} \cup \mathcal{E}_V} [\![\Phi]\!] \cdot [\![u]\!] \, ds,$$

and the functionals

$$F(\mathbf{w}) = 3 \int_\Omega \mathbf{Q}_1 \cdot \mathbf{w} \, d\mathbf{x}, \qquad G(u) = \int_\Omega Q_0 \, u \, d\mathbf{x}.$$

Then the method can be written as: find $(\mathbf{J}_h, \Phi_h) \in \mathbf{W}_h \times U_h$ such that

$$a(\mathbf{J}_h, \mathbf{w}) + b(\mathbf{w}, \Phi_h) = F(\mathbf{w}) \tag{3.3}$$
$$-b(\mathbf{J}_h, u) + c(\Phi_h, u) = G(u), \tag{3.4}$$

for all $(\mathbf{w}, u) \in \mathbf{W}_h \times U_h$. By setting

$$\mathcal{A}_h(\mathbf{J}, \Phi; \mathbf{w}, u) = a(\mathbf{J}, \mathbf{w}) + b(\mathbf{w}, \Phi) - b(\mathbf{J}, u) + c(\Phi, u)$$
$$\mathcal{H}(\mathbf{w}, u) = F(\mathbf{w}) + G(u),$$

we can formulate the method equivalently as: find $(\mathbf{J}_h, \Phi_h) \in \mathbf{W}_h \times U_h$ such that

$$\mathcal{A}_h(\mathbf{J}_h, \Phi_h; \mathbf{w}, u) = \mathcal{H}(\mathbf{w}, u)$$

for all $(\mathbf{w}, u) \in \mathbf{W}_h \times U_h$.

We note that the formulation (3.3)-(3.4) is well–posed (see [2, Proposition 2.1]) and consistent, due to the consistency of the numerical fluxes.

4. Error analysis. In this section, we present a priori error bounds for the DG method introduced in the previous section. Since this method belongs to the general class of DG methods analyzed in [2], the theoretical results there apply and give corresponding bounds for the method of Warsa, Wareing and Morel. For the sake of completeness, we review the abstract setting and the main steps of the analysis from [2].

As usual, we denote by $H^k(D)$, D being a domain in $\mathbb{R}^d$ or $\mathbb{R}^{d-1}$, the Sobolev spaces of integer orders, and by $\| \cdot \|_{k,D}$ the usual norms in $H^k(D)$ and $H^k(D)^d$. The following seminorm in $\mathbf{W} \times U$ can be naturally associated with the global form $\mathcal{A}_h$: $|(\mathbf{w}, u)|^2_{\mathcal{A}_h} := \mathcal{A}_h(\mathbf{w}, u; \mathbf{w}, u)$, for all $(\mathbf{w}, u) \in \mathbf{W} \times U$, i.e.,

$$|(\mathbf{w}, u)|^2_{\mathcal{A}_h} = 3 \|\sigma_t^{\frac{1}{2}} \, \mathbf{w}\|^2_{0,\Omega} + \|[\![\mathbf{w}]\!]\|^2_{0,\mathcal{E}_\mathcal{I} \cup \mathcal{E}_V} + 2 \|[\![\mathbf{w}]\!]\|^2_{0,\mathcal{E}_R} + \|\sigma_a^{\frac{1}{2}} \, u\|^2_{0,\Omega} + \frac{1}{4} \|[\![u]\!]\|^2_{\mathcal{E}_\mathcal{I} \cup \mathcal{E}_V}.$$

Whenever $\sigma_a > 0$, $|(\cdot, \cdot)|_{\mathcal{A}_h}$ actually defines a norm.

We assume that the local mesh sizes are of bounded variation, that is, there exists a constant $\ell > 0$ such that $\ell^{-1} h_K \le h_{K'} \le \ell h_K$, for all K and K' sharing a $(d-1)$–dimensional face. This assumption forbids the situation where the mesh is indefinitely

refined in only one of two adjacent subdomains, but allows for local refinement and is not restrictive in practice.

The main result is given in the following theorem.

THEOREM 4.1. *Assume the exact solution* $(\mathbf{J},\Phi)$ *of (2.1)–(2.2) to belong to* $H^{s+1}(\Omega)^d \times H^{s+2}(\Omega)$, *with* $s \geq 0$. *Let* $(\mathbf{J}_h,\Phi_h)$ *be the DG approximation, for an approximation degree* $k \geq 0$, *obtained on shape–regular meshes with possible hanging nodes and local mesh sizes of bounded variation. Then we have the error bound*

$$|(\mathbf{J}-\mathbf{J}_h,\Phi-\Phi_h)|_{\mathcal{A}_h} \leq C\, h^{\min\{s,k\}+\frac{1}{2}}\,(\|\mathbf{J}\|_{s+1,\Omega}+\|\Phi\|_{s+2,\Omega}),$$

with a constant $C>0$ *independent of the mesh size* h.
Furthermore, if the domain and the coefficients σ_t *and* σ_a *are sufficiently regular, we also have the* L^2*–bound*

$$\|\Phi-\Phi_h\|_{0,\Omega} \leq C\, h^{\min\{s,k\}+1}\,(\|\mathbf{J}\|_{s+1,\Omega}+\|\Phi\|_{s+2,\Omega}),$$

with a constant $C>0$ *independent of the mesh size* h.

REMARK 4.2. *The order of convergence in the approximation of the seminorm* $|(\cdot,\cdot)|_{\mathcal{A}_h}$ *is half a power of* h *better than for the standard LDG method, due to the stabilizing effect of the jump terms in the form* $a(\cdot,\cdot)$*; see [2]. Moreover, the above result also holds true for* $k=0$, *i.e., for piecewise constant approximations. For the LDG method, no convergence has been observed either theoretically or numerically in this case.*

REMARK 4.3. *The estimate of* $\|\Phi-\Phi_h\|_{0,\Omega}$ *is based on a standard duality argument and requires elliptic regularity. The exact requirement can be easily inferred from the proof of Theorem 4.1 outlined below.*

The proof of Theorem 4.1 follows from the abstract framework proposed in [2] and the theoretical results there. Here, we review the main steps of the analysis. First of all, we express the error $(\mathbf{e}_\mathbf{J},e_\Phi)=(\mathbf{J}-\mathbf{J}_h,\Phi-\Phi_h)$ as

$$(\mathbf{e}_\mathbf{J},e_\Phi)=(\mathbf{J}-\boldsymbol{\Pi}_h\mathbf{J},\Phi-\Pi_h\Phi_h)+(\boldsymbol{\Pi}_h\mathbf{J}-\mathbf{J}_h,\Pi_h\Phi-\Phi_h),$$

where $\boldsymbol{\Pi}_h$ and Π_h are the L^2–projections from $\mathbf{W}$ and U onto $\mathbf{W}_h$ and U_h, respectively. Then we make use of the following two ingredients:

(i) the so–called Galerkin orthogonality, which is a consequence of the consistency of the method:

$$\mathcal{A}_h(\mathbf{e}_\mathbf{J},e_\Phi;\mathbf{w},u)=0, \qquad \forall(\mathbf{w},u)\in\mathbf{W}_h\times U_h,$$

(ii) two inequalities that reflect the approximation properties of $\boldsymbol{\Pi}_h$ and Π_h, i.e.,

$$|\mathcal{A}_h(\mathbf{J}-\boldsymbol{\Pi}_h\mathbf{J},\Phi-\Pi_h\Phi_h;\mathbf{z}-\boldsymbol{\Pi}_h\mathbf{z},v-\Pi_h v)| \leq \mathcal{K}_1(\mathbf{J},\Phi;\mathbf{z},v),$$

for all $(\mathbf{J},\Phi),(\mathbf{z},v)\in\mathbf{W}\times U$, and

$$|\mathcal{A}_h(\mathbf{w},u;\mathbf{J}-\boldsymbol{\Pi}_h\mathbf{J},\Phi-\Pi_h\Phi_h)| \leq |(\mathbf{w},u)|_{\mathcal{A}_h}\,\mathcal{K}_2(\mathbf{J},\Phi),$$

for all $(\mathbf{w},u)\in\mathbf{W}_h\times U_h$ and $(\mathbf{J},\Phi)\in\mathbf{W}\times U$.

The error estimates of Theorem 4.1 can be obtained in terms of the functionals $\mathcal{K}_1$ and $\mathcal{K}_2$. In fact, the following result holds true (see [2, Lemma 2.3 and Lemma 2.4]).

LEMMA 4.4. *We have*

$$|(\mathbf{e}_\mathbf{J},e_\Phi)|_{\mathcal{A}_h} \leq \mathcal{K}_1^{\frac{1}{2}}(\mathbf{J},\Phi;\mathbf{J},\Phi)+\mathcal{K}_2(\mathbf{J},\Phi).$$

Moreover, if $(\mathbf{z}, v)$ *is the solution to the problem*

$$\nabla v + 3\,\sigma_t \mathbf{z} = \mathbf{0}, \qquad \nabla \cdot \mathbf{z} + \sigma_a v = e_\Phi, \tag{4.1}$$

with homogeneous boundary conditions $\frac{1}{4}v - \frac{1}{2}\mathbf{z}\cdot\mathbf{n} = 0$ *on* Γ_V *and* $\mathbf{z}\cdot\mathbf{n} = 0$ *on* Γ_R, *we have*

$$\|e_\Phi\|_{0,\Omega}^2 \le \mathcal{K}_1(\mathbf{J}, \Phi; -\mathbf{z}, v) + \mathcal{K}_2(\mathbf{J}, \Phi)\,\mathcal{K}_2(-\mathbf{z}, v).$$

Now, assume that $(\mathbf{J}, \Phi) \in H^{s+1}(\Omega)^d \times H^{s+2}(\Omega)$ and $(\mathbf{z}, v) \in H^{t+1}(\Omega)^d \times H^{t+2}(\Omega)$. From standard approximation properties of the L^2–projections, we can estimate the functional $\mathcal{K}_1$ in the first inequality of *(ii)* by

$$\mathcal{K}_1(\mathbf{J}, \Phi; \mathbf{z}, v) \le C\,h^{\min\{s,k\}+\min\{t,k\}+1}\,(\|\mathbf{J}\|_{s+1,\Omega} + \|\Phi\|_{s+2,\Omega})\,(\|\mathbf{z}\|_{t+1,\Omega} + \|v\|_{t+2,\Omega}),$$

with a constant $C > 0$ independent of the mesh size. Owing to the orthogonality properties of the L^2–projections, we can bound $\mathcal{K}_2$ in the second inequality of *(ii)* by

$$\mathcal{K}_2(\mathbf{J}, \Phi) \le C\,h^{\min\{s,k\}+\frac{1}{2}}\,(\|\mathbf{J}\|_{s+1,\Omega} + \|\Phi\|_{s+2,\Omega}),$$

with a constant $C > 0$ independent of the mesh size. The error estimate for $|(\mathbf{J} - \mathbf{J}_h, \Phi - \Phi_h)|_{\mathcal{A}_h}$ now immediately follows from the first part of Lemma 4.4, combined with the estimate for $\mathcal{K}_1$ for $(\mathbf{z}, v) = (\mathbf{J}, \Phi)$ and the one for $\mathcal{K}_2$.

To prove the L^2–error bound in Φ, let $(\mathbf{z}, v)$ be the solution of problem (4.1). We assume elliptic regularity, i.e., we assume that the domain and the coefficients are such that $(\mathbf{z}, v) \in H^1(\Omega)^d \times H^2(\Omega)$ and

$$\|\mathbf{z}\|_{1,\Omega} + \|v\|_{2,\Omega} \le C\|e_\Phi\|_{0,\Omega}, \tag{4.2}$$

with a constant $C > 0$ that only depends on the domain and the data. From the second part of Lemma 4.4 and the estimates of $\mathcal{K}_1$ and $\mathcal{K}_2$, we obtain

$$\|e_\Phi\|_{0,\Omega}^2 \le C\,h^{\min\{s,k\}+1}\,(\|\mathbf{J}\|_{s+1,\Omega} + \|\Phi\|_{s+2,\Omega})(\|\mathbf{z}\|_{1,\Omega} + \|v\|_{2,\Omega}).$$

Combining the above estimate with (4.2) yields the desired L^2–bound.

5. Numerical results. In this section, we present the results of a series of numerical experiments that demonstrate the theoretical error estimates of Theorem 4.1.

Example I: A smooth solution. We start by testing the performance of the method for a smooth solution. We consider the radiation–diffusion system (2.1) on $\Omega = (0,1)^3$, with reflecting boundary conditions on the faces $\{x = 0\}$ and $\{x = 1\}$, and vacuum boundary conditions on the remaining boundary faces. The material coefficients are $\sigma_t = 1$ and $\sigma_a = 10^{-4}$. The right–hand sides Q_0 and $\mathbf{Q}_1$ are chosen so that the exact solution $(\mathbf{J}, \Phi)$ is given by

$$\mathbf{J}(x,y,z) = \Big(x\,(1-x)\,y^2z^2,\; x^2(-y^2+y+1)(z-\tfrac{1}{2})^3,\; x^2(y-\tfrac{1}{2})^3(-z^2+z+1)\Big),$$
$$\Phi(x,y,z) = 16\,x^2\big(y-\tfrac{1}{2}\big)^3\big(z-\tfrac{1}{2}\big)^3.$$

This solution is arbitrarily smooth and allows us to test the theoretical convergence rates for polynomial approximation degrees $k = 0$ and $k = 1$.

Solutions are computed on a sequence of tetrahedral meshes $\{\mathcal{T}_i\}_{i=1}^5$ constructed by uniformly dividing the domain into Cartesian grids with 2^i, $i = 1, \ldots, 5$, equal intervals in each dimension. Each cube in the grid is then subdivided into six tetrahedra of equal volume. The mesh size h_i on mesh $\mathcal{T}_i$ is therefore proportional to 2^{-i}; specifically, $\{h_i\}_{i=1}^5 \simeq (4.33 \cdot 10^{-1}, 2.17 \cdot 10^{-1}, 1.08 \cdot 10^{-1}, 5.41 \cdot 10^{-2}, 2.71 \cdot 10^{-2})$.

In Table 5.1 we report the errors and estimates of the convergence rates in the $\mathcal{A}_h$–seminorm, in the L^2–norm of Φ, as well as in the L^2–norm of $\mathbf{J}$, for $k = 0$ and $k = 1$. If $e(\mathcal{T}_i)$ denotes the error (in the corresponding norm) on mesh $\mathcal{T}_i$, then

$$r_i = \frac{\log\big(e(\mathcal{T}_i)/e(\mathcal{T}_{i-1})\big)}{\log\big(h_i/h_{i-1}\big)}$$

is an estimate of the numerical convergence rate for $i > 1$. Clearly, convergence rates of 0.5 and 1.5 in the $\mathcal{A}_h$–seminorm, as well as order 1 and order 2 convergence in the L^2–norm for Φ, are obtained for $k = 0$ and $k = 1$, respectively. This confirms the theoretical results in Theorem 4.1. Also, the $\|\mathbf{J} - \mathbf{J}_h\|_{0,\Omega}$ part of the $\mathcal{A}_h$–seminorm actually converges more rapidly than the whole $\mathcal{A}_h$–seminorm. The $\|\mathbf{J} - \mathbf{J}_h\|_{0,\Omega}$ error converges with the optimal rates 1 and 2, for $k = 0$ and $k = 1$ respectively.

		$\lvert(\mathbf{J}-\mathbf{J}_h, \Phi-\Phi_h)\rvert_{\mathcal{A}_h}$		$\|\Phi-\Phi_h\|_{0,\Omega}$		$\|\mathbf{J}-\mathbf{J}_h\|_{0,\Omega}$	
	i	error	r_i	error	r_i	error	r_i
$k=0$	1	7.11 *e*–2	–	1.45 *e*–2	–	3.13 *e*–2	–
	2	4.91 *e*–2	5.34 *e*–1	8.90 *e*–3	7.00 *e*–1	1.90 *e*–2	7.18 *e*–1
	3	3.21 *e*–2	6.14 *e*–1	4.71 *e*–3	9.17 *e*–1	1.02 *e*–2	9.04 *e*–1
	4	2.14 *e*–2	5.82 *e*–1	2.40 *e*–3	9.73 *e*–1	5.21 *e*–3	9.67 *e*–1
	5	1.47 *e*–2	5.47 *e*–1	1.21 *e*–3	9.90 *e*–1	2.63 *e*–3	9.87 *e*–1
$k=1$	1	4.40 *e*–2	–	7.22 *e*–3	–	1.21 *e*–2	–
	2	1.91 *e*–2	1.20 *e*+0	2.36 *e*–3	1.61 *e*+0	3.71 *e*–3	1.71 *e*+0
	3	7.41 *e*–3	1.36 *e*+0	6.33 *e*–4	1.90 *e*+0	9.78 *e*–4	1.92 *e*+0
	4	2.74 *e*–3	1.43 *e*+0	1.61 *e*–4	1.97 *e*+0	2.47 *e*–4	1.99 *e*+0
	5	9.91 *e*–4	1.47 *e*+0	4.06 *e*–5	1.99 *e*+0	6.16 *e*–5	2.00 *e*+0

TABLE 5.1

Smooth solution: errors and convergence rates r_i in the $\mathcal{A}_h$–seminorm, L^2–norm of Φ and L^2–norm of $\mathbf{J}$, for $k = 0, 1$.

The convergence behavior of the different jump contributions to the $\mathcal{A}_h$–seminorm is shown in Figure 5.1 for $k = 0$. In the legend, the abbreviations I, R and V are used for $\mathcal{E}_\mathcal{I}$, $\mathcal{E}_R$ and $\mathcal{E}_V$, respectively. Comparison with the line $y = n^{-1/2}$ clearly shows that the jumps over interior faces, $\|[\![\mathbf{J}_h]\!]\|_{0,\mathcal{E}_\mathcal{I}} = \|[\![\mathbf{J} - \mathbf{J}_h]\!]\|_{0,\mathcal{E}_\mathcal{I}}$ and $\|[\![\Phi]\!]\|_{0,\mathcal{E}_\mathcal{I}} = \|[\![\Phi - \Phi_h]\!]\|_{0,\mathcal{E}_\mathcal{I}}$, converge with rates of $\mathcal{O}(h^{\frac{1}{2}})$. On the other hand, comparison with the line $y = n^{-1}$ shows that all the boundary jumps exhibit $\mathcal{O}(h^1)$ convergence. Results for the case $k = 1$ are presented in Figure 5.2. Comparing the jump errors with the lines $y = n^{-1}$ and $y = n^{-3/2}$ indicates that the interior jumps converge with rates of $\mathcal{O}(h^{\frac{3}{2}})$ while the boundary jump terms exhibit $\mathcal{O}(h^2)$ convergence.

Example II: A piecewise smooth solution. In this second example, we consider a piecewise smooth solution. As in the first example, we have $\Omega = (0, 1)^3$, this time with with vacuum boundary conditions on the faces $\{x = 0\}$ and $\{x = 1\}$, and reflecting boundary conditions on the remaining boundary faces. The material coefficients are $\sigma_t = 1$ and $\sigma_a = 0$ and the right–hand sides Q_0 and $\mathbf{Q}_1$ are chosen such

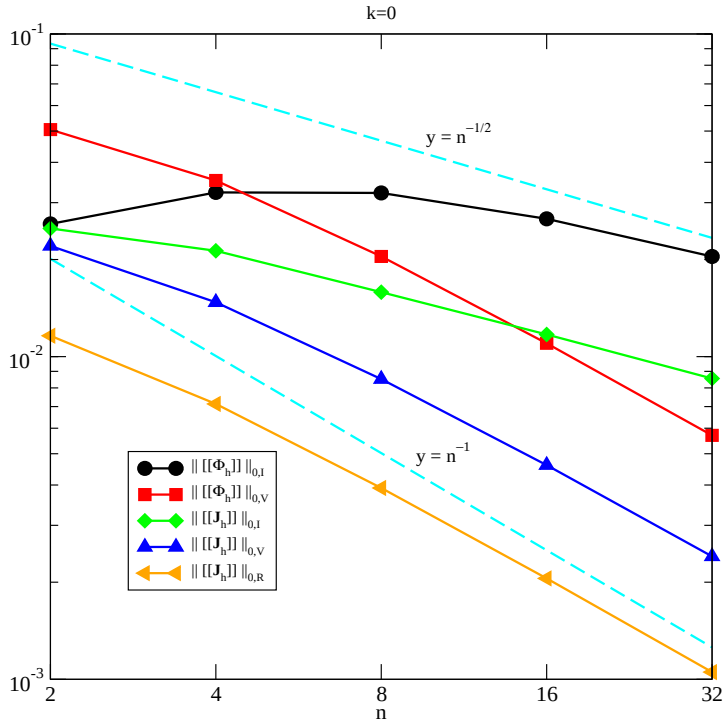

FIG. 5.1. *Smooth solution: L^2-errors of the jumps in* $\mathbf{J}$ *and* Φ*, for* $k = 0$.

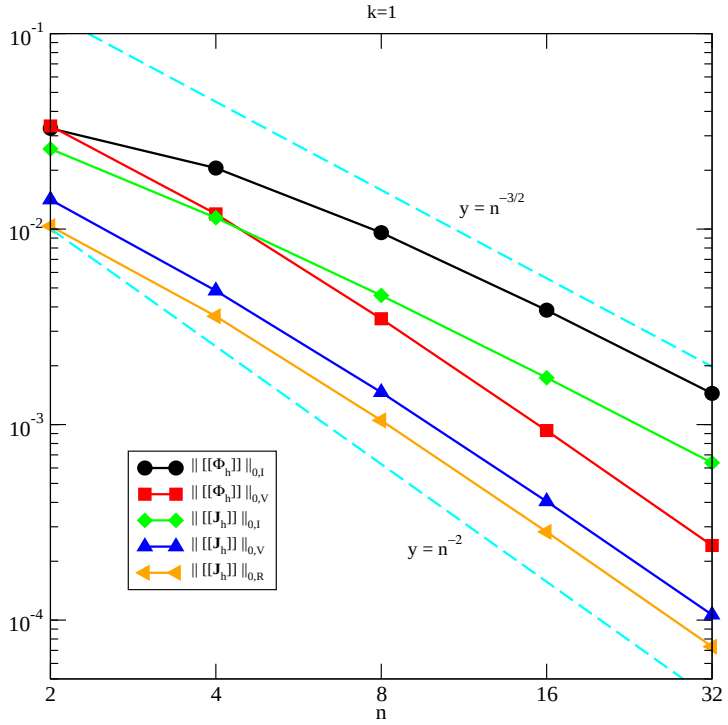

FIG. 5.2. *Smooth solution: L^2-errors of the jumps in* $\mathbf{J}$ *and* Φ*, for* $k = 1$.

that the exact solution is

$$\mathbf{J}(x,y,z) = \Big(\tfrac{1}{8}x + (x-\tfrac{1}{2})y^2z^2,\, 0,\, 0\Big),$$
$$\Phi(x,y,z) = \begin{cases} y^2z^2 & \text{in } (0,0.5)\times(0,1)\times(0,1), \\ y^2z^2 + (x-\tfrac{1}{2})^2 & \text{in } (0.5,1)\times(0,1)\times(0,1). \end{cases}$$

Since the coefficients σ_t and σ_a are constant and the domain is convex, the elliptic regularity assumptions for problem (4.1) are satisfied. Notice that Φ belongs to $H^{\frac{5}{2}-\varepsilon}(\Omega)$, $\varepsilon > 0$, but is piecewise polynomial. One would therefore expect a deterioration in the convergence rates for $k = 1$ as a direct consequence of Theorem 4.1. However, the proof of Theorem 4.1 can be straightforwardly adapted to *piecewise* smooth solutions, and the same convergence rates as in Example I are predicted. This is confirmed in the numerical results reported in Table 5.2, for the same sequence of meshes as in Example I. The rates $k+\frac{1}{2}$ in the $\mathcal{A}_h$–seminorm and $k+1$ in the L^2–norms of Φ and $\mathbf{J}$ are clearly seen. Furthermore, the jump errors exhibit the same convergence rates as in Example I and so the corresponding plots are not shown for this problem.

		$\lvert(\mathbf{J}-\mathbf{J}_h, \Phi-\Phi_h)\rvert_{\mathcal{A}_h}$		$\lVert\Phi-\Phi_h\rVert_{0,\Omega}$		$\lVert\mathbf{J}-\mathbf{J}_h\rVert_{0,\Omega}$	
	i	error	r_i	error	r_i	error	r_i
$k=0$	1	2.56 e–1	–	1.12 e–1	–	7.31 e–2	–
	2	1.94 e–1	4.01 e–1	5.80 e–2	9.56 e–1	4.26 e–2	7.79 e–1
	3	1.42 e–1	4.55 e–1	2.93 e–2	9.85 e–1	2.32 e–2	8.80 e–1
	4	1.02 e–1	4.78 e–1	1.47 e–2	9.94 e–1	1.21 e–2	9.36 e–1
	5	7.24 e–2	4.89 e–1	7.36 e–3	9.98 e–1	6.19 e–3	9.67 e–1
$k=1$	1	1.07 e–1	–	2.16 e–2	–	1.73 e–2	–
	2	4.10 e–2	1.39 e+0	5.46 e–3	1.98 e+0	4.58 e–3	1.92 e+0
	3	1.49 e–2	1.46 e+0	1.37 e–3	2.00 e+0	1.16 e–3	1.98 e+0
	4	5.34 e–3	1.48 e+0	3.42 e–4	2.00 e+0	2.92 e–4	1.99 e+0
	5	1.90 e–3	1.49 e+0	8.55 e–5	2.00 e+0	7.32 e–5	2.00 e+0

TABLE 5.2

Piecewise smooth solution: errors and convergence rates r_i in $\mathcal{A}_h$–seminorm, L^2–norm of Φ and L^2–norm of $\mathbf{J}$, for $k = 0, 1$.

Example III: A two–material problem. In practice, the coefficient σ_t may have strong discontinuities at the interfaces between different materials. In these cases, where the vector-valued fluxes $\frac{1}{3\sigma_t}\nabla\Phi$ and $\mathbf{J}$ are typically smoother than the scalar flux Φ, the use of mixed methods, as the one proposed in this paper, is of particular importance. In this example, we will consider this kind of situation, where the radiation–diffusion equations (2.1) are solved with $\sigma_a = 0$ and a discontinuous coefficient σ_t. We again set $\Omega = (0,1)^3$, and set vacuum boundary conditions on the faces $\{x = 0\}$ and $\{x = 1\}$ with reflecting boundary conditions on the remaining boundary faces. We define $\sigma_t = a$, for $0 \le x \le 0.5$, $\sigma_t = b$, for $0.5 < x \le 1$, with positive parameters a and b, modeling a material discontinuity at $x = 0.5$. The right–hand sides $\mathbf{Q}_1$ and Q_0 are chosen so that the solution $(\mathbf{J}, \Phi)$ is given as follows. Denoting by $\varphi(y,z)$ the polynomial $\varphi(y,z) = y^2z^2$, define

$$\mathbf{J}(x,y,z) = \Big(\tfrac{3}{4}\big(a + x(b-a)\big)\cdot\varphi(y,z),\, 0,\, 0\Big),$$
$$\Phi(x,y,z) = \begin{cases} 3a(x-\tfrac{1}{2})\varphi(y,z) & \text{in } (0,0.5)\times(0,1)\times(0,1), \\ 3b(x-\tfrac{1}{2})\varphi(y,z) & \text{in } (0.5,1)\times(0,1)\times(0,1). \end{cases}$$

Notice that Φ is again piecewise smooth, but only belongs to $H^{\frac{3}{2}-\varepsilon}(\Omega)$, $\varepsilon > 0$, whereas the vector fluxes $\mathbf{J}$ and $\frac{1}{3\sigma_t}\nabla\Phi = \Big(\varphi(y,z), (x-\frac{1}{2})\partial_y\varphi(y,z), (x-\frac{1}{2})\partial_z\varphi(y,z)\Big)$ are smooth functions. For the numerical calculations, we use the same sequence of tetrahedral meshes as in the previous examples.

We consider the two cases $a = 1$, $b = 0.01$ and $a = 100$, $b = 1$. Notice that the jump in the normal derivative of Φ at the surface $x = 0.5$ is equal to $3(a-b)y^2z^2$. This jump is of almost two orders of magnitude larger in the case $a = 100$, $b = 1$ than in the case $a = 1$, $b = 0.01$. For this reason, deterioration of the convergence rates due to the lack of smoothness of the exact solution might be more serious in the second case than in the first one.

For the case $a = 1$, $b = 0.01$, we show in Table 5.3 the errors and the convergence rate estimates in the $\mathcal{A}_h$–seminorm and in the L^2–norm of Φ, as well as in the L^2-norm of $\mathbf{J}$, for $k = 0$ and $k = 1$. Orders 0.5 and 1.5 convergence in the $\mathcal{A}_h$–seminorm, and order 1 and 2 convergence in the L^2–norm for Φ, for $k = 0$ and $k = 1$, respectively, are obtained. These results agree with the theoretical estimates in Theorem 4.1, as in the previous two examples, even though the elliptic regularity assumptions of Theorem 4.1 for the estimate of the L^2–error in Φ are not satisfied. Furthermore, the L^2–error in $\mathbf{J}$ also converges with the optimal orders 1 and 2, for $k = 0$ and $k = 1$, respectively.

		$\lvert(\mathbf{J}-\mathbf{J}_h, \Phi-\Phi_h)\rvert_{\mathcal{A}_h}$		$\lVert\Phi-\Phi_h\rVert_{0,\Omega}$		$\lVert\mathbf{J}-\mathbf{J}_h\rVert_{0,\Omega}$	
	i	error	r_i	error	r_i	error	r_i
$k=0$	1	1.76 e–1	–	6.15 e–2	–	5.14 e–2	–
	2	1.27 e–1	4.67 e–1	3.18 e–2	9.50 e–1	2.92 e–2	8.17 e–1
	3	8.95 e–2	5.04 e–1	1.61 e–2	9.85 e–1	1.54 e–2	9.21 e–1
	4	6.30 e–2	5.08 e–1	8.07 e–3	9.95 e–1	7.91 e–3	9.61 e–1
	5	4.44 e–2	5.05 e–1	4.04 e–3	9.98 e–1	4.01 e–3	9.80 e–1
$k=1$	1	9.42 e–2	–	1.59 e–2	–	1.39 e–2	–
	2	3.66 e–2	1.36 e+0	4.06 e–3	1.97 e+0	3.56 e–3	1.97 e+0
	3	1.33 e–2	1.46 e+0	1.02 e–3	1.99 e+0	8.73 e–4	2.03 e+0
	4	4.77 e–3	1.49 e+0	2.55 e–4	2.00 e+0	2.13 e–4	2.04 e+0
	5	1.69 e–3	1.49 e+0	6.38 e–5	2.00 e+0	5.26 e–5	2.02 e+0

TABLE 5.3

Two-material problem, $a = 1$, $b = 0.01$: errors and convergence rates r_i in $\mathcal{A}_h$–seminorm, L^2–norm of Φ and L^2–norm of $\mathbf{J}$, for $k = 0, 1$.

In Figures 5.3 and 5.4, the errors in the jumps of Φ and $\mathbf{J}$ for $k = 0$ and $k = 1$, respectively, are shown. As in Example I, we see that the interior jumps converge at the rates $\mathcal{O}(h^{\frac{1}{2}})$ and $\mathcal{O}(h^{\frac{3}{2}})$ for $k = 0$ and $k = 1$, respectively, while the boundary jumps show the full convergence rate of $\mathcal{O}(h^1)$ and $\mathcal{O}(h^2)$, for $k = 0$ and $k = 1$, respectively.

Consider now the case $a = 100$, $b = 1$. The numerical rates in Table 5.4 indeed show a different picture than the previous case of $a = 1$ and $b = 0.01$. For both $k = 0$ and $k = 1$, the rates in the $\mathcal{A}_h$–seminorm have deteriorated slightly, but they are still close to 0.5 and 1.5, for $k = 0$ and $k = 1$, respectively. Similar behavior is observed in the L^2–norm of $\mathbf{J}$. These results are in agreement with Theorem 4.1. The differences in the L^2–errors in Φ are more remarkable: the convergence rates are smaller than 0.5 for $k = 0$ and better than 2 for $k = 1$.

Finally, we show in Figures 5.5 and 5.6 the behavior of the errors in the jumps of Φ and $\mathbf{J}$ for $k = 0$ and $k = 1$, respectively. For $k = 0$, the jumps of Φ on the reflective

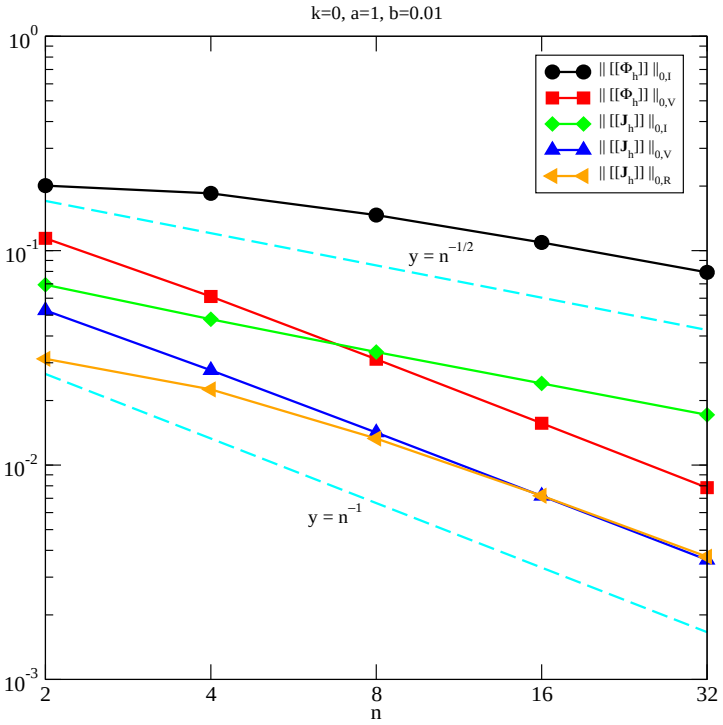

FIG. 5.3. *Two-material problem, $a = 1$, $b = 0.01$: L^2-errors of the jumps in $\mathbf{J}$ and Φ, for $k = 0$.*

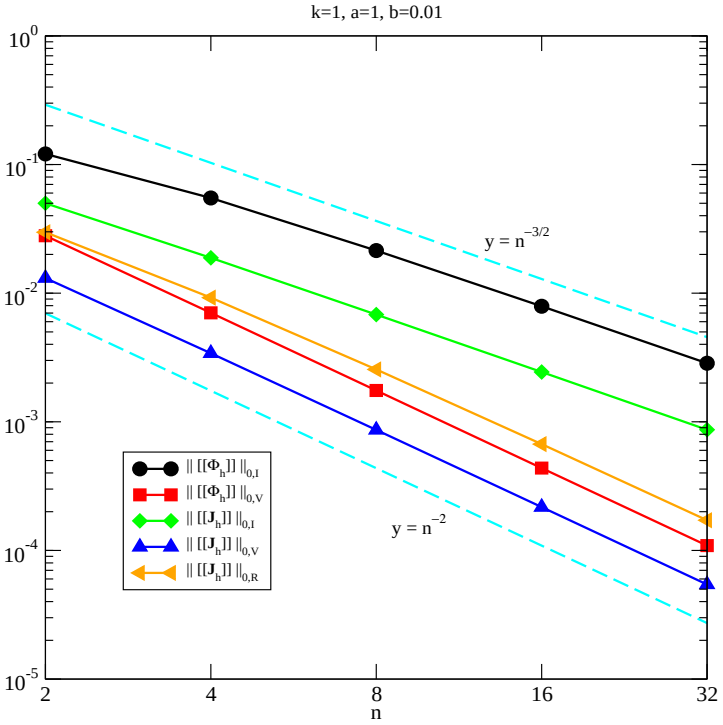

FIG. 5.4. *Two-material problem, $a = 1$, $b = 0.01$: L^2-errors of the jumps in $\mathbf{J}$ and Φ, for $k = 1$.*

		$\lvert(\mathbf{J}-\mathbf{J}_h, \Phi-\Phi_h)\rvert_{\mathcal{A}_h}$		$\lVert\Phi-\Phi_h\rVert_{0,\Omega}$		$\lVert\mathbf{J}-\mathbf{J}_h\rVert_{0,\Omega}$	
	i	error	r_i	error	r_i	error	r_i
$k=0$	1	1.47 e+1	–	7.76 e+0	–	3.83 e+0	–
	2	1.05 e+1	4.84 e–1	5.05 e+0	6.21 e–1	2.01 e+0	9.29 e–1
	3	7.49 e+0	4.90 e–1	3.49 e+0	5.34 e–1	1.04 e+0	9.56 e–1
	4	5.32 e+0	4.95 e–1	2.59 e+0	4.29 e–1	5.33 e–1	9.57 e–1
	5	3.79 e+0	4.87 e–1	1.94 e+0	4.17 e–1	2.78 e–1	9.42 e–1
$k=1$	1	5.36 e+0	–	2.68 e+0	–	8.23 e–1	–
	2	2.09 e+0	1.36 e+0	6.91 e–1	1.95 e+0	2.17 e–1	1.92 e+0
	3	8.44 e–1	1.31 e+0	1.56 e–1	2.14 e+0	5.72 e–2	1.93 e+0
	4	3.43 e–1	1.30 e+0	3.35 e–2	2.22 e+0	1.53 e–2	1.90 e+0
	5	1.36 e–1	1.33 e+0	7.37 e–3	2.19 e+0	4.15 e–3	1.88 e+0

TABLE 5.4

Two-material problem, $a = 100$, $b = 1$: errors and convergence rates r_i in $\mathcal{A}_h$–seminorm, L^2–norm of Φ and L^2–norm of $\mathbf{J}$, for $k = 0, 1$.

boundary in this case converge more slowly – and suboptimally – than the case $a = 1$, $b = 0.01$, while the other jumps exhibit rates of convergence similar to those for the case $a = 1$, $b = 0.01$. For $k = 1$, the jumps of Φ on the reflective boundary exhibit convergence similar to those for $k = 0$. However, here convergence is at the optimal rate of $\mathcal{O}(h^{\frac{3}{2}})$ that is, half an order less than the L^2-norm. All the other jumps show a convergence rates as for the $k = 0$ case.

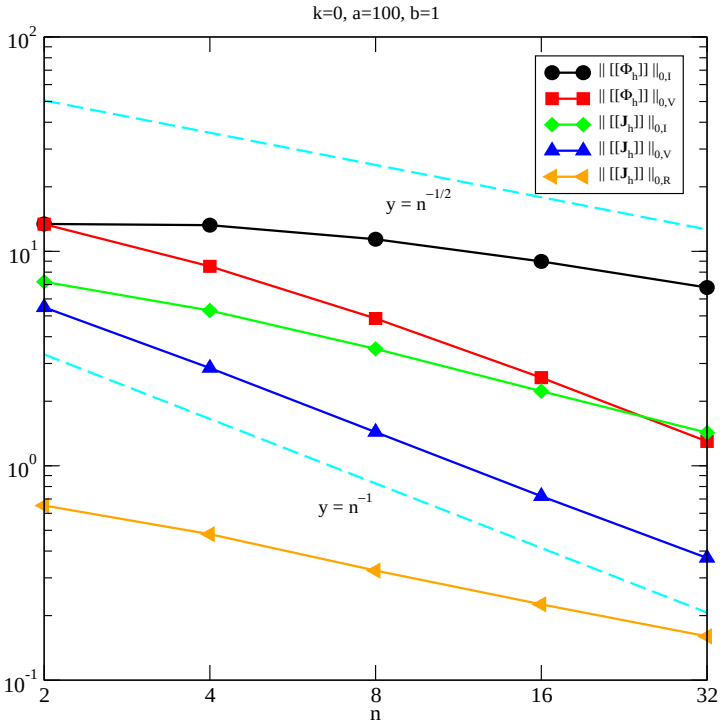

FIG. 5.5. *Two-material problem, $a = 100$, $b = 1$: L^2-errors of the jumps in $\mathbf{J}$ and Φ, for $k = 0$.*

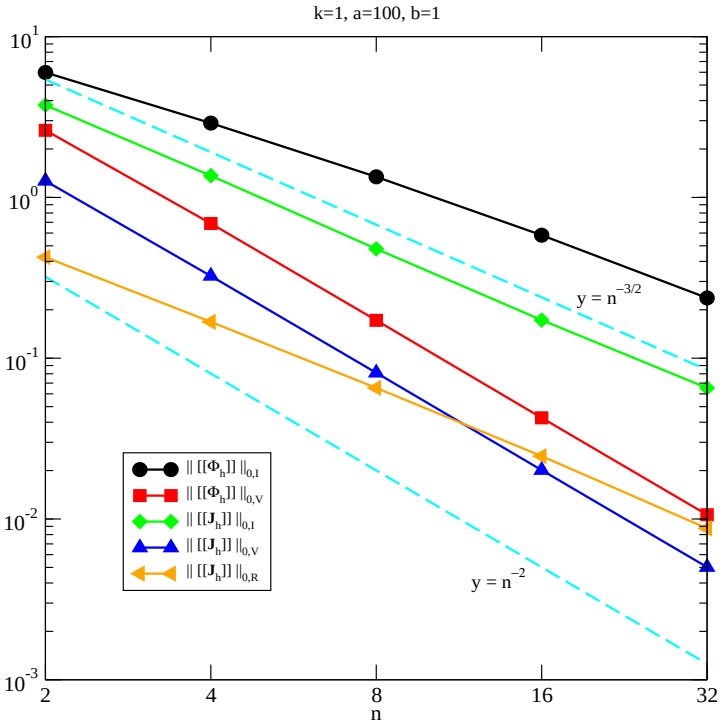

FIG. 5.6. *Two-material problem, $a = 100$, $b = 1$: L^2-errors of the jumps in $\mathbf{J}$ and Φ, for $k = 1$.*

6. Conclusions. The discontinuous Galerkin method of Warsa, Wareing and Morel introduced in [12] and [11] for two– and three–dimensional domains, respectively, is a mixed finite element method used to compute numerical solutions for problems of radiation–diffusion. That method belongs to the general class of mixed DG methods presented and analyzed in [2]. The analysis there guarantees that, for polynomial approximation degrees $k \geq 0$, the method converges with order $k + \frac{1}{2}$ in the vector unknown and with order $k + 1$ in the scalar unknown. The numerical experiments we presented confirm that these rates are sharp.

Acknowledgments. The authors would like to thank Michele Benzi of Emory University for bringing this collaboration together. They would also like to thank Jim Morel and Todd Wareing of Los Alamos National Laboratory.

REFERENCES

[1] D. ARNOLD, F. BREZZI, B. COCKBURN, AND L. MARINI, *Unified analysis of discontinuous Galerkin methods for elliptic problems*, SIAM J. Numer. Anal., 39 (2001), pp. 1749–1779.

[2] P. CASTILLO, B. COCKBURN, I. PERUGIA, AND D. SCHÖTZAU, *An a priori error analysis of the local discontinuous Galerkin method for elliptic problems*, SIAM J. Numer. Anal., 38 (2000), pp. 1676–1706.

[3] B. COCKBURN, *Discontinuous Galerkin methods for convection-dominated problems*, in High-Order Methods for Computational Physics, T. Barth and H. Deconink, eds., vol. 9 of Lect. Notes Comput. Sci. Engrg., Springer–Verlag, 1999, pp. 69–224.

[4] B. COCKBURN, G. KANSCHAT, I. PERUGIA, AND D. SCHÖTZAU, *Superconvergence of the local discontinuous Galerkin method for elliptic problems on Cartesian grids*, SIAM J. Numer. Anal., 39 (2001), pp. 264–285.

[5] B. Cockburn, G. Karniadakis, and C.-W. Shu, eds., *Discontinuous Galerkin Methods. Theory, Computation and Applications*, vol. 11 of Lect. Notes Comput. Sci. Engrg., Springer–Verlag, 2000.

[6] B. Cockburn and C.-W. Shu, *The local discontinuous Galerkin method for time–dependent convection–diffusion systems*, SIAM J. Numer. Anal., 35 (1998), pp. 2440–2463.

[7] ———, *Runge–Kutta discontinuous Galerkin methods for convection–dominated problems*, J. Sci. Comp., 16 (2001), pp. 173–261.

[8] B. Davison, *Neutron Transport Theory*, Clarendon Press, 1957.

[9] E. E. Lewis and J. W. F. Miller, *Computational Methods of Neutron Transport*, American Nuclear Society, 1993.

[10] I. Perugia and D. Schötzau, *An hp-analysis of the local discontinuous Galerkin method for diffusion problems*, J. Sci. Comp., 17 (2002), pp. 561–571.

[11] J. Warsa, T. Wareing, and J. Morel, *Fully consistent diffusion synthetic acceleration of linear discontinuous transport discretizations on three-dimensional unstructured meshes*, Nucl. Sci. Engrg., (2002). To appear.

[12] ———, *Solution of the discontinuous P_1 equations in two-dimensional Cartesian geometry with two-level preconditioning*, SIAM J. Sci. Comput., (2002). To appear.

[13] J. S. Warsa, M. Benzi, T. A. Wareing, and J. E. Morel, *Preconditioning a mixed discontinuous finite element method for radiation diffusion*, Numer. Lin. Alg. Appl., (2001). Submitted.